Evaluation of ERA-Interim and MERRA Cloudiness in the Southern Ocean

CATHERINE M. NAUD AND JAMES F. BOOTH*

Applied Physics and Applied Mathematics, Columbia University, New York, New York

ANTHONY D. DEL GENIO

NASA Goddard Institute for Space Studies, New York, New York

(Manuscript received 22 July 2013, in final form 4 November 2013)

ABSTRACT

The Southern Ocean cloud cover modeled by the Interim ECMWF Re-Analysis (ERA-Interim) and Modern-Era Retrospective Analysis for Research and Applications (MERRA) reanalyses are compared against Moderate Resolution Imaging Spectroradiometer (MODIS) and Multiangle Imaging Spectroradiometer (MISR) observations. ERA-Interim monthly mean cloud amounts match the observations within 5%, while MERRA significantly underestimates the cloud amount. For a compositing analysis of clouds in warm season extratropical cyclones, both reanalyses show a low bias in cloud cover. They display a larger bias to the west of the cyclones in the region of subsidence behind the cold fronts. This low bias is larger for MERRA than for ERA-Interim. Both MODIS and MISR retrievals indicate that the clouds in this sector are at a low altitude, often composed of liquid, and of a broken nature. The combined *CloudSat–Cloud–Aerosol Lidar and Infrared Pathfinder Satellite Observations* (*CALIPSO*) cloud profiles confirm these passive observations, but they also reveal that low-level clouds in other parts of the cyclones are also not properly represented in the reanalyses. The two reanalyses are in fairly good agreement for the dynamic and thermodynamic characteristics of the cyclones, suggesting that the cloud, convection, or boundary layer schemes are the problem instead. An examination of the lower-tropospheric stability distribution in the cyclones from both reanalyses suggests that the parameterization of shallow cumulus clouds may contribute in a large part to the problem. However, the differences in the cloud schemes and in particular in the precipitation processes, which may also contribute, cannot be excluded.

1. Introduction

Recently, Trenberth and Fasullo (2010) reported that most general circulation models (GCMs) that participated in the Coupled Model Intercomparison Project phase 3 (CMIP3) overestimated solar absorption in the Southern Ocean and that this was accompanied by a lack of clouds in this region. Haynes et al. (2011) determined that the two main cloud regimes affecting the shortwave radiation in the region are 1) frontal clouds because they are highly reflective, and 2) low-level clouds because they are ubiquitous. Bodas-Salcedo et al. (2012) found that the model they tested had difficulties producing low- and midlevel clouds in the cold sector of Southern Hemisphere (SH) extratropical cyclones, which had a significant effect on the shortwave radiation in the SH oceans. Similarly, a collection of GCMs run in hindcast mode also displayed errors in surface shortwave absorption in extratropical cyclones (Williams et al. 2013), which was due to cloud cover deficiencies behind the cold fronts.

Here we investigate if this low bias in Southern Ocean cloud cover is also present in reanalyses, which are models that assimilate multiple observations and as such are deemed more reliable. The two reanalyses we examine are the Interim European Centre for Medium-Range Weather Forecasts (ECMWF) Re-Analysis (ERA-Interim; Dee et al. 2011) and the National Aeronautics and Space Administration (NASA) Modern-Era Retrospective Analysis for Research and Applications (MERRA; Rienecker et al. 2011). For this task, we use a variety of observations from the NASA *Terra* and the A-Train: the

Denotes Open Access content.

*Current affiliation: Earth and Atmospheric Sciences, City College of New York, New York, New York.

Corresponding author address: Catherine M. Naud, Applied Physics and Applied Mathematics, Columbia University, 2880 Broadway, New York, NY 10025.
E-mail: cn2140@columbia.edu

DOI: 10.1175/JCLI-D-13-00432.1

Terra Moderate Resolution Imaging Spectroradiometer (MODIS; Salomonson et al. 1989), the Multiangle Imaging Spectroradiometer (MISR; Diner et al. 1998), the Advanced Microwave Scanning Radiometer for Earth Observing System (AMSR-E; Kawanishi et al. 2003), the Atmospheric Infrared Sounder (AIRS; Aumann et al. 2003), *CloudSat* (Stephens et al. 2002), and the *Cloud–Aerosol Lidar and Infrared Pathfinder Satellite Observations* (*CALIPSO*; Winker et al. 2009).

Our investigation focuses on clouds in extratropical cyclones during the warm season, when the shortwave errors reported by Trenberth and Fasullo (2010) are greatest. This task is conducted using a cyclone-centered compositing technique as in Naud et al. (2006), Field and Wood (2007), Field et al. (2008), and Naud et al. (2012), to only cite a few. This technique allows us to relate biases to specific atmospheric conditions because cyclones include ascending and descending, warm and cold, and wet and dry regions, and help pinpoint the type of problem a model might have. The variety in observations also allows a better characterization of cloud properties and distribution. In this paper, we will first discuss the differences between observations and the two reanalyses in monthly mean cloud cover, then move on to discuss differences specific to extratropical cyclones.

2. Data and methods

This section summarizes the observations and reanalysis output used in this evaluation and the method for cyclone-centered compositing. Monthly means for 30°–70°S are first checked using data for the years 2002–11. For the extratropical cyclone study the period is reduced to 2006–10 to accommodate the length of the *CloudSat* and *CALIPSO* missions. This encompasses four warm seasons [November–March (NDJFM)] for the Southern Hemisphere midlatitudes. Finally, we use observations at the temporal and spatial resolution of the satellite measurements (level 2) as well as data products that have been gridded and temporally averaged (level 3).

a. Observations and reanalysis

For monthly cloud cover observations, we use two instruments: the MODIS 1° × 1° gridded monthly mean cloud fractions from the level-3 MODIS *Terra* files (MOD08; Platnick et al. 2003), and the MISR Cloud Fraction by Altitude (CFbA; Di Girolamo et al. 2010) 0.5° × 0.5° gridded monthly cloud fractions.

For cloud observations near coincident with cyclone detections, we use three different datasets: the MODIS MOD08 daily files, the MISR CFbA daily files, and the *CloudSat–CALIPSO* joint product geometric profile "GEOPROF-LIDAR" (Mace et al. 2009). The MODIS retrievals used here are the cloud fraction and the cloud-top thermodynamic phase, pressure, and temperature. The MISR CFbA files provide total cloud fractions. We also collected the MISR level-2 files that provide the stereo cloud-top heights and cloud-top winds ("TC-CLOUD"; Moroney et al. 2002). Finally, the combined *CloudSat–CALIPSO* GEOPROF-LIDAR files provide cloud vertical distribution information.

To identify the cyclones, the modeling, analysis, and prediction (MAP) climatology of midlatitude storminess (MCMS; Bauer and Del Genio 2006) database of extratropical cyclone locations and tracks obtained with ERA-Interim sea level pressure fields is used. For cyclone monthly frequency of occurrence, we use MCMS data for years 2000–10. For collocating the cyclones with cloud observations, we use MCMS data from 2006 to 2010. Note that we use the term cyclone to refer to a snapshot of a storm event, rather than the full life cycle of the storm.

The AMSR-E retrievals of precipitable water (PW) are available in the level-2 ocean product files (Wentz and Meissner 2004) and collected for the period 2006–10. These retrievals are not available over land or sea ice, and the implications will be discussed in section 6.

ERA-Interim and MERRA monthly total cloud cover are collected for 2002–11 and averaged in their native grids (1.5° × 1.5° and 0.667° × 0.5°, respectively). In addition, 6-hourly total cloud cover, skin temperature, PW, boundary layer height, sea level pressure, and vertical profiles of winds, vertical velocities, geopotential heights, temperature, and cloud cover are collected for the 2006–10 time period for both reanalyses. The reanalyses do not provide cloud outputs generated with the Cloud Feedback Model Intercomparison Project (CFMIP) Observation Simulator Package (COSP) simulators (Bodas-Salcedo et al. 2011). The assimilation system and observations used by the two reanalyses are described in Dee et al. (2011) for ERA-Interim and Rienecker et al. (2011) for MERRA, and neither directly assimilates cloud observations. The two reanalyses share a similar assimilation process and similar observations, as discussed in Rienecker et al. (2011). For the Southern Ocean most of these observations are ships, buoys, and satellite data. There are some differences though—for example, ERA-Interim assimilates global positioning system data but MERRA does not, while MERRA includes more of the Advanced Microwave Sounding Unit-A (AMSU-A) channels than ERA-Interim (Rienecker et al. 2011). In any case, both reanalyses were improved in the southern midlatitudes in terms of their precipitation, column-integrated precipitable water, clouds, and indirectly surface and top-of-the-atmosphere radiation, when microwave observations, only assimilated over the oceans, were included (Bosilovich et al. 2011).

b. Methods

For each cyclone, we extract MISR and MODIS daily cloud cover observations, MISR level-2 stereo heights and winds, AMSR-E PW, and all of the reanalysis outputs that were obtained on the same day (or the same time for reanalysis) within 25° of the cyclone's center (defined by the point of minimum sea level pressure). For daily observations, the time delay between the cyclone detection and the cloud observations can be up to 24 h, while for the level-2 MISR and AMSR-E products, we restrict the time difference to within 3 h. These observations and reanalysis outputs are then projected onto a cyclone-centered stereographic grid where cells are equidistant from the center (100-km radial and 14.4° angular resolutions). No rotation is applied before we average all the cyclone grids together. The impact of such a rotation has little influence on our results as we are looking mostly at differences between similarly obtained composites. For presentation purposes, we flip all composites along the north–south direction, so that the pole is at the top of the figures and the equator at the bottom (as in, e.g., Field and Wood 2007). Again, this choice has no impact on the results. The compositing method of the data is extensively described in Naud et al. (2012, 2013) and Booth et al. (2013). The impact of uncertainties in the method and the observations on the total cloud cover cyclone-centered composites is extensively discussed in Naud et al. (2013) who find that the overall uncertainty in MISR and MODIS composites is about 5%. Consequently, differences between model and observations less than 5% are not considered significant nor discussed.

We also construct composites along vertical transects at two locations within the cyclones: 1) across warm fronts and 2) along a segment 7.5° west of the low pressure centers confined between −10° and 10° of the latitude of the low pressure centers. These vertical grids are 1° resolution along the horizontal and 250-m resolution along the vertical. These are used to composite the vertical distribution of cloud cover for data from *CloudSat–CALIPSO* observations and output from both ERA-Interim and MERRA. For the transect across warm fronts, the method is identical to the one used in Naud et al. (2010, 2012) and Booth et al. (2013), where warm fronts are located following a method by Hewson (1998) applied to MERRA 850-mb potential temperatures. Here, because of the near coincidence between the reanalysis outputs and observations, the cloud outputs from the reanalysis are extracted along the *CloudSat* orbit, for those cyclones with a warm front successfully located and with an intersect between the orbit and the front. For the 7.5°W segment, however, all the cloud outputs are used, whether a *CloudSat* orbit intersected this region of the cyclone or not. Consequently, the sample size in terms of number of cyclones is smaller for the observations than models.

A total of 21 000 cyclones is used for the cyclone-centered composites that use daily observations and reanalysis, 80% of which also have an AMSR-E coincidence and 60% have a MISR level-2 coincidence. The number of cyclones that contribute to the vertical transects is reduced by the requirement that *CloudSat–CALIPSO* orbits intersect a warm front and is found to be around 1200. The MISR observations are only available during the daytime, while both MODIS and *CloudSat–CALIPSO* cloud observations are performed during both day- and nighttime.

3. Southern Ocean cloud cover

MODIS, MISR, and reanalysis 10-yr-average cloud cover maps are shown in Fig. 1. Because MISR cloud observations are only available during daytime, we checked differences between daytime-only and day and night MODIS cloud cover. We find that MODIS daytime-only cloud cover over open ocean and north of 60°S can be up to 0.04 greater than the combined daytime and nighttime cloud cover. However, south of 60°S, daytime cloud cover is larger by 0.1, while over Antarctica it is 0.3 lower. This difference in the MODIS day and night cloud cover is most certainly caused by issues in cloud detection over bright surfaces at night when the algorithm is only using thermal channels (e.g., Ackerman et al. 2008). We show day and night cloud cover for MODIS, ERA-Interim, and MERRA in Fig. 1, but keep in mind that MODIS cloud cover may be underestimated when sea ice is present.

MODIS and MISR agree fairly well that cloud cover in the Southern Ocean exceeds 0.8 in a band between 40° and 60°S, with a narrower band with fractions in excess of 0.9 between about 50° and 60°S (Figs. 1a,b). The fractions in the MISR set are less uniform. This is the result of a number of differences between the two products: the MISR monthly products are at higher resolution than the MODIS products, and MISR has a narrower instrument swath and daytime-only observations, and thus smaller coverage and sampling. There are some differences between the two datasets; for example, regions of greater than 0.95 cloud cover are more extensive in the MODIS dataset, but overall the two datasets are within 0.05 of each other.

The ERA-Interim reanalysis (Fig. 1c) underestimates cloud cover by about 0.1 (i.e., it does not fully reproduce the extent of the region of greater than 0.9 cloud cover when compared to MODIS). This error is greater

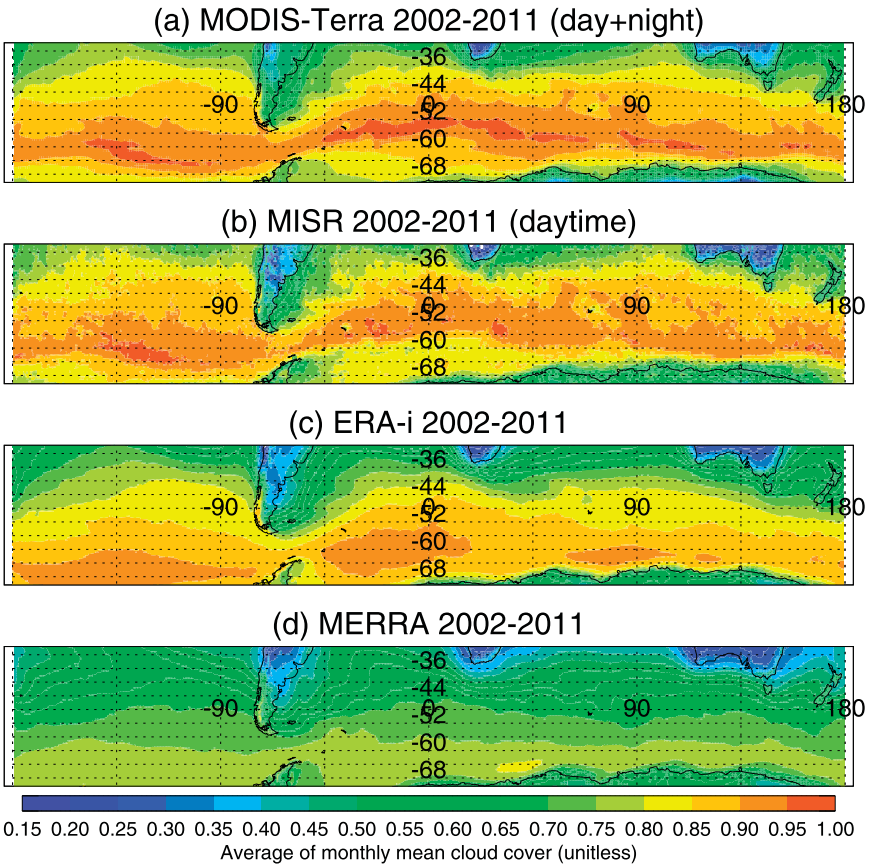

FIG. 1. A 10-yr 2002–11 average of monthly cloud cover from (a) MODIS *Terra*, (b) MISR CFbA, (c) ERA-Interim (ERA-i), and (d) MERRA.

equatorward of 60°S, while poleward of 60°S ERA-Interim has a larger cloud cover. Cloud retrievals are difficult over snow and sea ice when using passive instruments, thus this overestimate is probably not revealing of issues with the reanalysis but of issues with the observations. In fact, combined radar and lidar *CloudSat–CALIPSO* austral winter cloud cover reaches 0.9 to 0.95 in the 60°–70°S band (Mace et al. 2009). In contrast, the MERRA cloud cover (Fig. 1d) is significantly lower than the observations in the entire region, with a difference of at least 0.2 where cloud cover is observed to be at its maximum.

The impact of the cloud cover underestimate on top-of-the-atmosphere radiative fluxes would be an overestimate in the longwave and an underestimate in the shortwave outgoing fluxes for both reanalyses. A preliminary comparison with Clouds and the Earth's Radiant Energy System Energy Balanced and Filled (CERES-EBAF) top-of-the-atmosphere fluxes (Loeb et al. 2009) indicates that this is indeed the case for both reanalyses, at least north of 60°S where cloud observations are more reliable and the bias is more robust. However, we find that the shortwave biases in the two reanalyses are of the same order even though cloud biases in MERRA are significantly larger. One possible reason, which we intend to explore further in a separate study, is that MERRA cloud optical thicknesses are much larger than observed or produced in ERA-Interim.

One important factor for cloud presence in this region is the large number of extratropical cyclones. According to the MCMS database, a cyclone travels through a region of approximately 1000 km × 1000 km every 3 days on average (Fig. 2). Hodges et al. (2011) report that the location and intensity of extratropical cyclones are fairly consistent between modern reanalyses; thus, we want to examine how the two reanalyses perform for their cloud cover in extratropical cyclones.

4. Cloud cover in observations and reanalyses: SH warm season extratropical cyclones

We average cloud observations in a stereographic grid centered on the point of minimum pressure within the cyclones. We remind the reader that the composites are

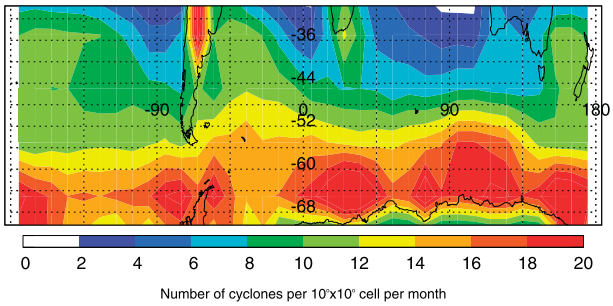

FIG. 2. Number of extratropical cyclone centers that are present in a 10° × 10° box per month averaged over 2000–10.

flipped along the north–south direction. Thus, to describe the northern part of the cyclones we will use the phrase ''equatorward'' instead and for the southern part, ''poleward.'' For comparison with MODIS cloud cover, ERA-Interim and MERRA cloud cover are selected for both day- and nighttime cyclones, but for comparison with MISR, only daytime cloud covers are composited.

As shown in Fig. 3, the cloud cover maxima tend to occur in the region where warm fronts are found and in the wrap-around region at the cyclone center. Equatorward of the center, cloud covers are lower (i.e., 0.7–0.8). Both MODIS (Fig. 3a) and MISR (Fig. 3b) retrievals give very similar spatial distributions, despite the inclusion of nighttime observations in the MODIS composites.

The ERA-Interim composite of total cloud cover gives a spatial distribution similar to the observations (Fig. 3c), with a maximum from the low pressure center poleward and eastward along the warm frontal zone, and lower fractions equatorward than poleward. However, with the exception of the warm frontal zone and poleward edge, ERA-Interim cloud cover is 0.05–0.14 lower than observed (Figs. 4a,b). The differences between ERA-Interim and MODIS and MISR are small on the poleward half of the cyclones, but both MODIS and MISR cloud cover datasets are less certain when snow- or sea ice–covered land are present in this region of the cyclones (Naud et al. 2013). Consequently, we are unable to evaluate ERA-Interim cloud cover accuracy in this region of the cyclones. The differences with MISR are larger on the equatorward half of the cyclone when compared to those with MODIS. MISR cloud cover was found to be larger than both MODIS and *CloudSat–CALIPSO* in the equatorward-east quadrant of the cyclones (Naud et al. 2013); therefore, the magnitude of the cloud cover bias in that region is less certain. Nevertheless, both observational datasets indicate a tendency for ERA-Interim to underestimate cloud cover to the west of the low pressure center.

The MERRA composite of total cloud cover clearly displays more substantial biases (Fig. 3d). Except for a fairly reduced region where the warm fronts should be, MERRA cloud cover is less than 0.7 in most of the cyclone region (Fig. 3d), with differences greater than 0.2 to the west of the low, relative to MODIS and MISR (Figs. 4c,d). The results shown in Fig. 4 highlight two problems: 1) both reanalyses display a bias in cyclone cloud cover that is largest in the region west of the low center, and 2) the magnitude of the biases is different between the two reanalyses. To address the first problem, we investigate the observed cloud properties distribution within the cyclones to characterize the type of clouds that causes the largest biases. To address the second problem, we investigate if there are inherent differences between the two reanalyses, first in their representation of the large-scale characteristics of the cyclones (dynamics, moisture availability) and second in their ability to simulate clouds (parameterizations).

5. Cloud properties in SH cyclones

In this section, we work to determine the details of the cyclones' clouds to better understand what physical processes might be deficient in the reanalyses. Therefore, we use MODIS and MISR cloud property retrievals to characterize the cloud types within the cyclones, and we use *CloudSat–CALIPSO* cloud profiles to characterize the vertical structure of these clouds.

a. Cyclone-centered observed cloud-top properties

Figure 5a shows the MODIS composite of cloud-top pressure. The region of the cyclone that has the lowest cloud-top pressures coincides with the warm frontal zone and extends into the warm sector, on the equatorward side, to the east of the low pressure center. On the western side of the cyclones, in the cold sector at the back of the cold fronts, on average cloud-top pressures are at least 680 hPa.

MODIS cloud-top temperatures reflect this west–east contrast but also show the signature of the meridional temperature gradient (Fig. 5b). The warmest cloud tops are found in the warm sector, equatorward and to the east of the low pressure center, but wraparound the low to the west and extend into the poleward side of the cyclones. Consequently, the coldest cloud tops are confined to the poleward east quadrant.

The MISR cloud-top height composite (Fig. 5c) is similar to that of the MODIS cloud-top pressures. The highest cloud tops are along the warm frontal zone and extend equatorward to the east, while low-level clouds are found to the west and extend poleward, with an average cloud-top height below 3 km.

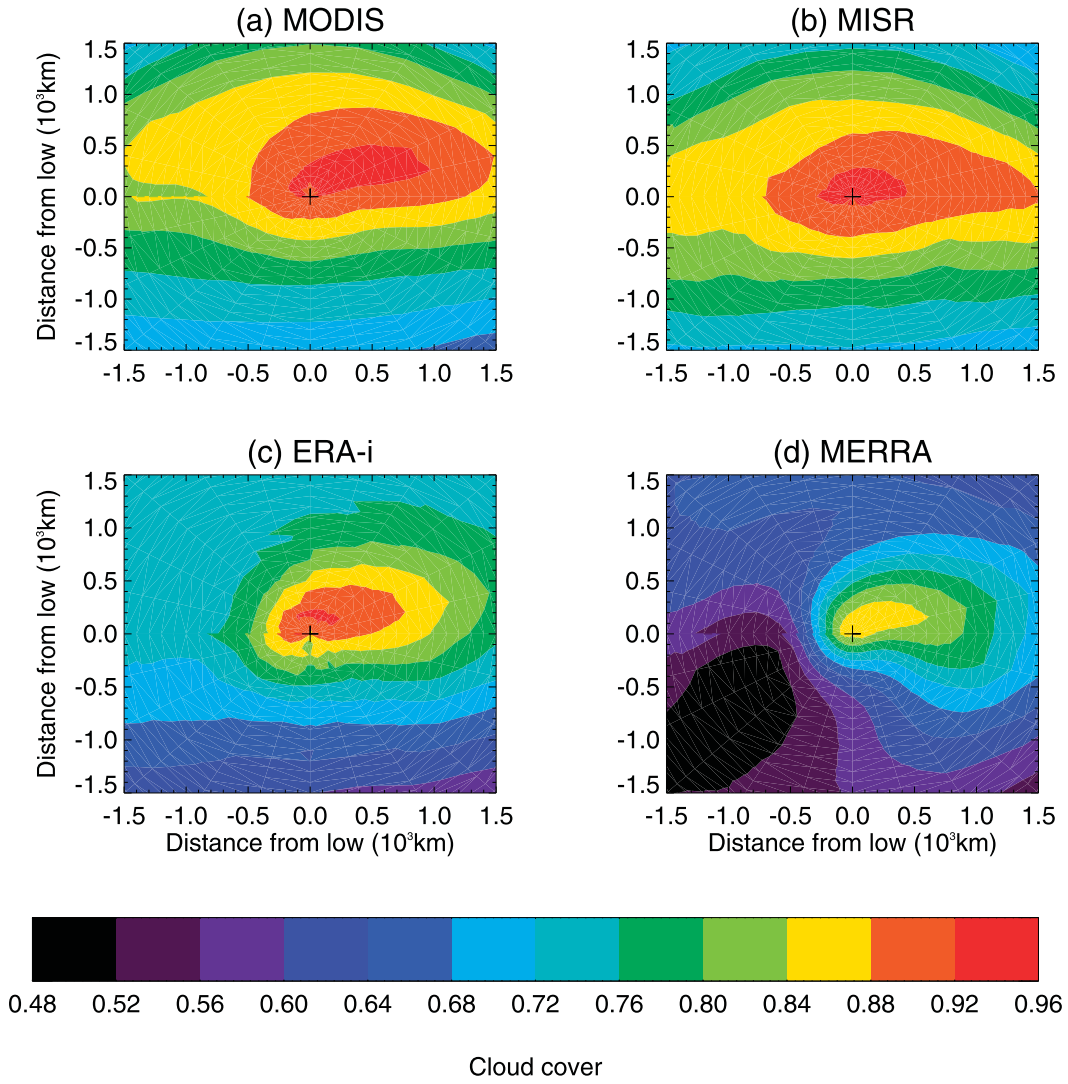

FIG. 3. Cyclone-centered composites of cloud cover in the Southern Hemisphere warm season for (a) MODIS, (b) MISR, (c) ERA-Interim (ERA-i), and (d) MERRA.

Cloud-top thermodynamic phase is also retrieved with MODIS for 1-km cloudy pixels that are used in the microphysics retrieval routine in daytime granules only (Platnick et al. 2003). The daily files provide liquid, ice, and "undetermined" phase (when the algorithm does not reach a definite identification) cloud fractions, but only for pixels that are entirely cloud covered. In this case, liquid (or ice or undetermined) cloud fraction is the number of times liquid is identified at cloud top divided by the total number of daytime cloudy and clear observations. A significant difference between this cloud fraction product and the one we have used so far is that partially filled pixels are now considered as clear. Consequently, this total cloud fraction (all phases included) is lower than that in Fig. 3a.

Figure 6 shows the MODIS cloud cover composites for each phase (liquid, ice, and undetermined) defined as the number of one phase occurrence divided by the total number of clear and cloudy pixels. On average, liquid clouds occur most often in the poleward west quadrant (Fig. 6a), while ice clouds occur predominantly in the warm frontal zone and into the warm sector (Fig. 6b). In the west-equatorward sector, liquid fraction is less than farther poleward, while ice fractions are the lowest. Thus, in this quadrant, undetermined phase or partially filled/clear pixels must occur more often than in the poleward west quadrant. Figure 6c shows that the undetermined phase does not occur very often. We calculated the occurrence of partially filled pixels as the difference between the total cloud cover shown in Fig. 3a minus the

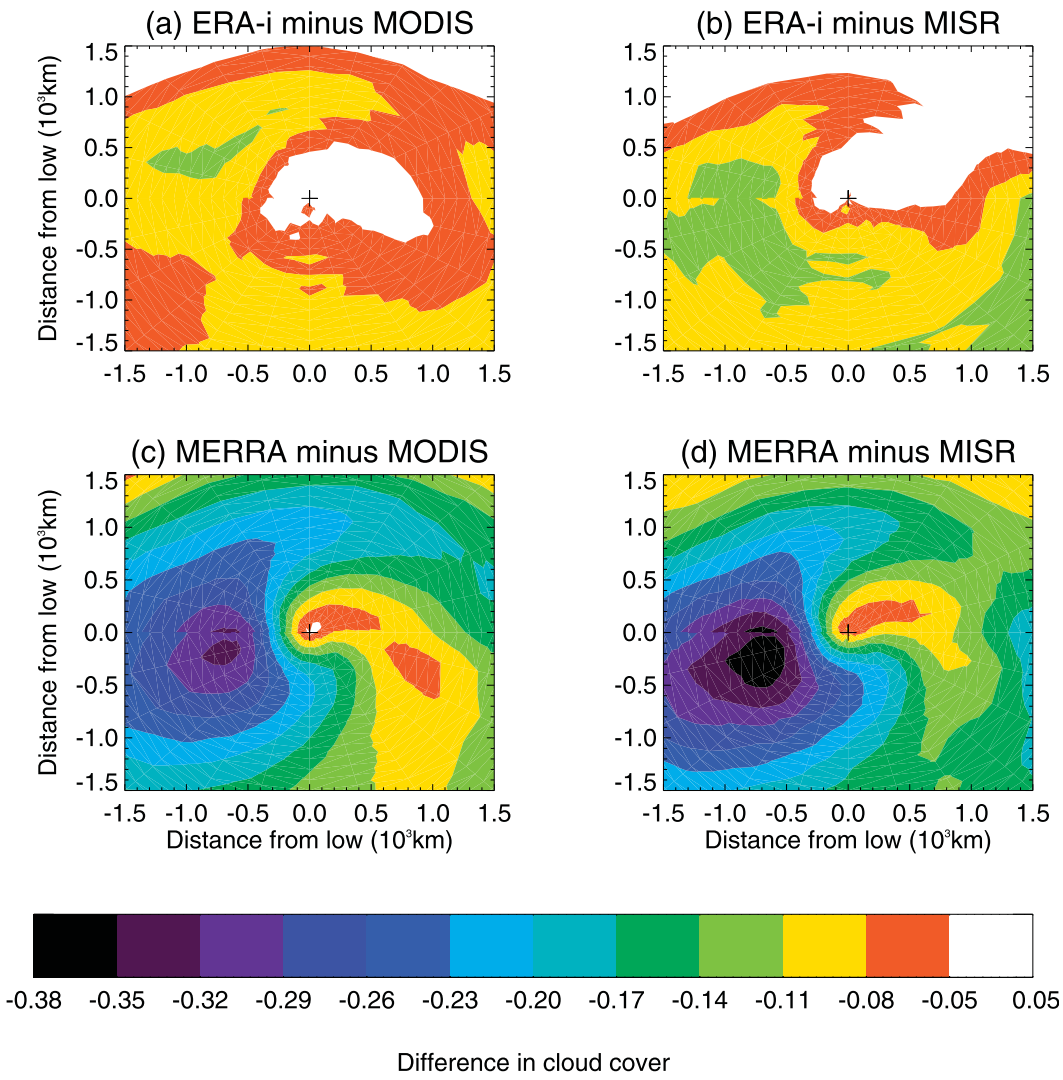

FIG. 4. Difference in cyclone-centered composites of SH warm season cloud cover between (a) ERA-Interim (ERA-i) and MODIS, (b) daytime ERA-Interim and MISR, (c) MERRA and MODIS, and (d) daytime MERRA and MISR.

total cloud cover obtained as the sum of liquid, ice, and undetermined cloud cover. Figure 6d shows that partially filled pixels occur most often in the equatorward-west quadrant. Consequently, this region of the cyclones must contain a relatively large occurrence of broken clouds.

These cloud properties composites suggest that the western side of the cyclones (where ERA-Interim and MERRA underestimate cloud cover the most) is a region populated predominantly by low level, with relatively warm tops, and often liquid broken clouds. Next, we use *CloudSat–CALIPSO* vertical profiles of cloud locations to evaluate if low-level clouds are indeed at the root of the problem for the reanalysis products.

b. Comparison of cloud cover vertical distributions

MODIS and MISR may misclassify some of the optically thin high-altitude clouds as mid- or low-level clouds. Also, when averaging together cloud-top pressures or heights, information on the distributions is lost and the dominant cloud level may not match the average. Therefore, we want to ensure that low-level clouds (with a top within the first 3 km above the surface) are the real problem. The *CloudSat–CALIPSO* combined cloud retrievals provide more accurate detections of optically thin clouds (Mace et al. 2009). Therefore, we use *CloudSat–CALIPSO* vertical profiles of cloud location to composite vertical transects of cloud cover in

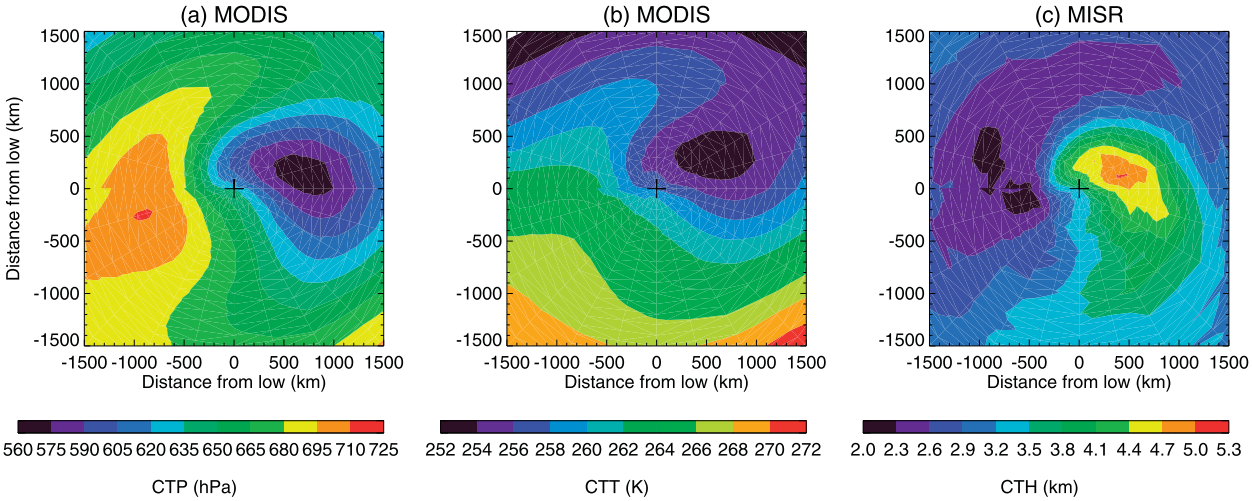

FIG. 5. Cyclone-centered composite of SH warm season (a) MODIS cloud-top pressure (CTP), (b) MODIS cloud-top temperature (CTT), and (c) MISR cloud-top height (CTH).

two different regions of the cyclones: 1) across the warm front as in Naud et al. (2010; 2012) and 2) 7.5° west of the low pressure center (along a line from −10° to +10° from the latitude of the low).

Figure 7 shows the observed cloud vertical distribution across warm fronts using *CloudSat–CALIPSO* (Fig. 7a), ERA-Interim (Fig. 7b), and MERRA (Fig. 7c) cloud vertical profiles. As described by Naud et al. (2010, 2012) for winter cyclones, clouds are mostly found along the frontal tilt, with a secondary maximum at low level across the entire transect (Fig. 7a). Precipitating droplets cannot be distinguished from cloud droplets in the radar signal (e.g., Marchand et al. 2008), and this may overestimate cloud fractions near the surface by about 10% (Naud et al. 2010). As was the case in the map view composites, the ERA-Interim cloud vertical distribution (Fig. 7b) slightly underestimates the cloud cover (0.2 less), while MERRA greatly underestimates the cloud cover (0.4 less; Fig. 7c). These underestimates are larger than the uncertainty introduced by precipitation contamination in the observations.

Figure 8 shows analogous composites of cloud vertical cover along a segment positioned 7.5° to the west of the low pressure centers, between −10° and 10° of the latitude of the low pressure centers. In this region of the cyclones, clouds are found mostly at low altitudes, as the maximum in cloud cover is below 3 km (Fig. 8a). This verifies that the average cloud level given in Fig. 5 is consistent with the vertical cloud distribution. Cloud cover in this lower band is less than 0.6, so these clouds are not present all the time or are broken clouds. In addition, we note a reduction in cloud cover from the poleward to the equatorward sections of the transects (from right to left in Fig. 8a). The ERA-Interim cloud vertical transect (Fig. 8b) resembles the observations. However, the maximum cloud cover in the lowest 2 km is less than 0.4. The MERRA cloud vertical transect (Fig. 8c) also resembles the observations. However, the maximum cloud cover in the lowest band is even less than ERA-Interim, mostly below 0.3.

The *CloudSat* radar is not reliable in the first kilometer of the atmosphere, as surface clutter is large and thus can mask or be confused with cloud signal. According to Marchand et al. (2008) and Mace et al. (2009), the radar cloud mask takes this problem into account, and the files used here should not have a rate of false cloud detection larger than 5%. In addition, the lidar on board *CALIPSO* does not have this problem and in regions where only low-level clouds are present, even if they may attenuate the lidar, their cloud top will be detected. Consequently, this comparison of cloud profiles taken together with the comparison with MODIS and MISR strongly suggests low-level cloud cover deficiencies in both ERA-Interim and MERRA.

6. SH warm season cyclone characteristics

Now that we have established that both ERA-Interim and MERRA underestimate cyclone cloud cover and that this difference is largest where low-level clouds are predominant, we investigate if this is caused by differences in the cyclone circulation or thermodynamics or by issues in the parameterizations involved in cloud formation. For this we compare dynamic and thermodynamic variables for the two reanalyses. Since the largest biases occurred to the west of the low center, we

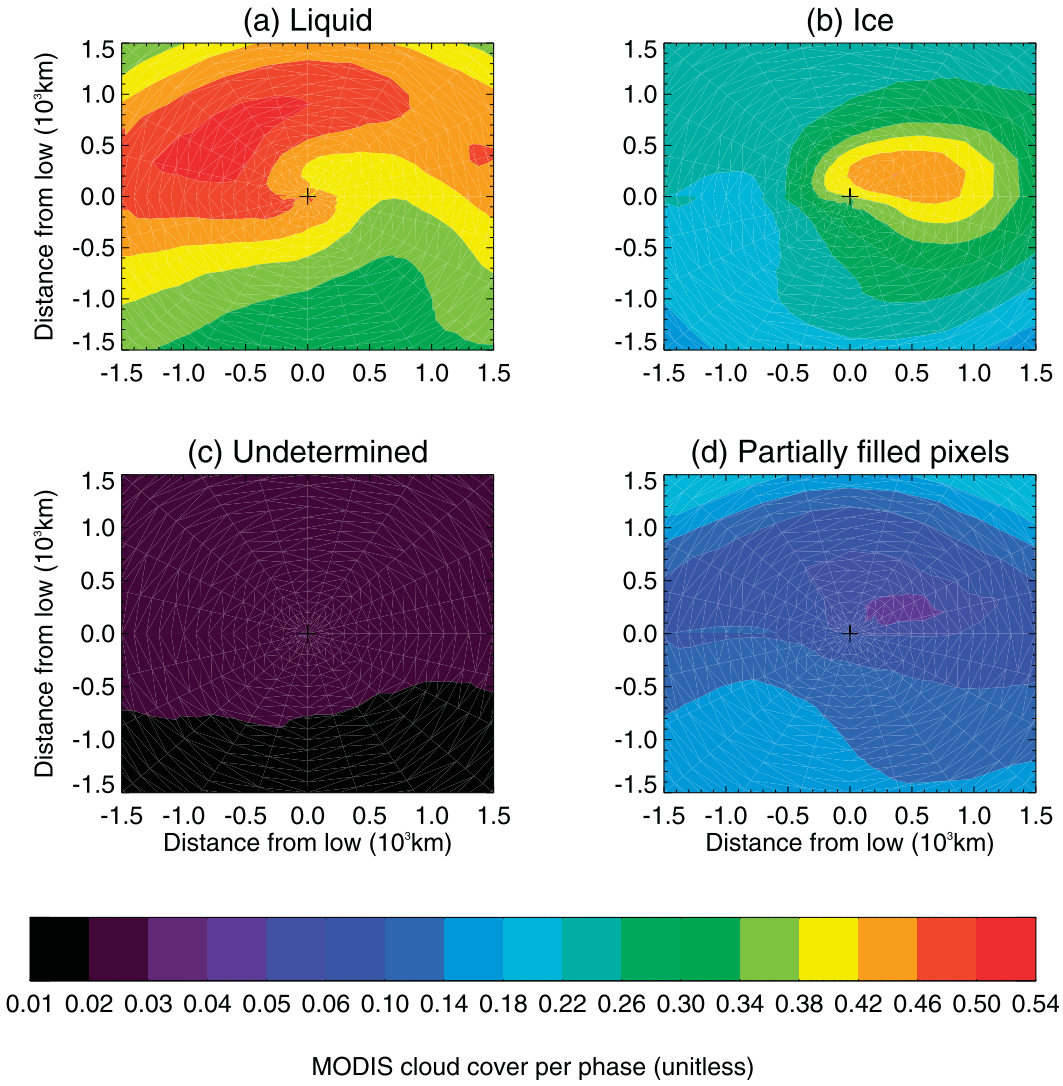

FIG. 6. Cyclone-centered composites of SH warm season MODIS cloud cover per thermodynamic phase for (a) liquid, (b) ice, and (c) undetermined cloud phase (number of given phase detections divided by the total number of clear and cloudy detections), and (d) fraction of partially filled pixels (total cloud cover minus the sum of all three phases cloud cover).

focus on this region. We note that the western region of the cyclone is on average a region of subsidence, with colder temperatures, lower moisture amounts, and lower precipitation than east of the low (e.g., Bauer and Del Genio 2006).

a. Cyclones dynamics and thermodynamics characteristics

First we examine the cyclone-centered composites of 850-hPa horizontal winds. Figure 9c shows the difference between MERRA and ERA-Interim 850-hPa wind composites. For most of the cyclone area, the difference between the two reanalyses is within 0.5 m s^{-1}, with the exception of a small region poleward of the low pressure center, where MERRA winds are slightly more vigorous by up to 2 m s^{-1}. The distribution of the differences does not correlate with the difference in cloud cover. To verify that the winds in the two reanalyses are realistic, we also show the winds retrieved at cloud top from MISR, when cloud-top heights are below 3 km (Fig. 9b). The overall distribution of the wind speeds and the location of the maximum are very similar between ERA-Interim (Fig. 9a) and MISR (Fig. 9b), with MISR winds slightly stronger as they can be sometimes assigned to higher levels than 850 hPa.

We then compared the moisture content of the cyclones in both reanalyses to AMSR-E PW (Fig. 10a). Both ERA-Interim (Fig. 10b) and MERRA (Fig. 10c)

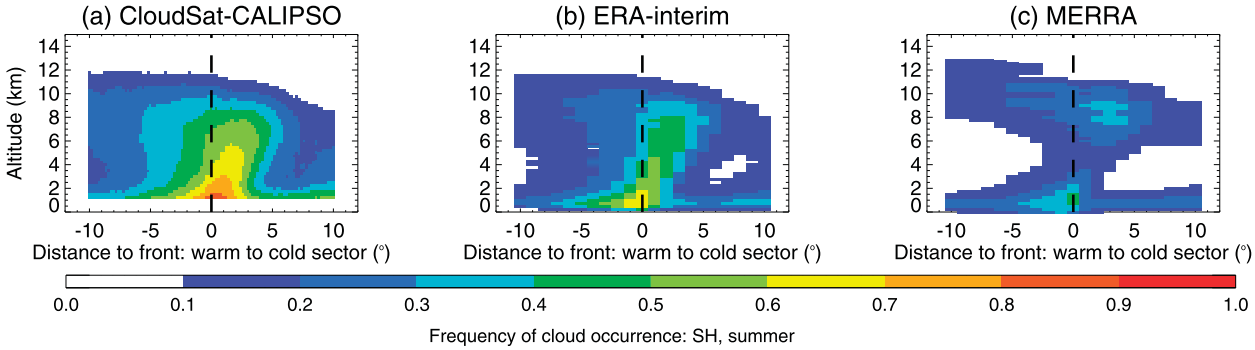

FIG. 7. Composites of cloud vertical distribution along a perpendicular to the warm front, for warm season SH cyclones, in (a) *CloudSat–CALIPSO* observations, (b) ERA-Interim, and (c) MERRA.

slightly overestimate PW (mostly less than 2 mm) equatorward of the low but underestimate PW poleward of the low by up to 6 mm. This causes a larger moisture gradient than observed, but it does not spatially correlate with the region of greatest underestimate in cloud cover found in the comparison with MODIS and MISR. In addition, AMSR-E PW is not retrieved when sea ice is present or over land, which may cause a bias on the polar side of the cyclones. However, a MERRA composite of PW created using only columns where no sea ice is present shows no change in the poleward PW values (not shown).

Finally, we compared ERA-Interim and MERRA vertical velocity at 850 hPa (Fig. 11). For both reanalyses (Figs. 11a,b), a large ascent zone (with negative values meaning upward motions) is seen to the east and poleward of the low, and extends into the warm sector (equatorward and east). In contrast, the western side of the low shows on average a subsidence zone, with a maximum (positive down), slightly toward the equator. These patterns are identical to those described by Bauer and Del Genio (2006). The two reanalyses slightly differ on the poleward edge of the cyclones, with more vigorous subsidence in ERA-Interim than MERRA. This difference is small and does not exceed 1 hPa h^{-1}. Also, the maximum ascent at the low is more vigorous in ERA-Interim than MERRA, but with differences less than 3 hPa h^{-1}. The spatial distribution and range of vertical velocities are overall very similar between the two reanalyses, and no correlation in the difference is found with the difference in cloud cover.

Differences in dynamics or thermodynamics between the two reanalyses would not be surprising in the Southern Ocean where sources of assimilated data may differ and may also be sparse. Moreover, the cyclone detection is performed with ERA-Interim sea level pressure outputs, which entails that not all cyclones in this database occur in MERRA. In fact, Hodges et al. (2011) report that about 83% of ERA-Interim cyclones have a match in MERRA during the warm season. However, we find that the large-scale moisture, horizontal winds, and the vertical motions within extratropical cyclones are very similar between the two reanalysis. In addition, our results show that the largest differences are found for a specific cloud type in a specific region of the cyclones. Therefore, errors in both reanalysis cloud fields may have to be attributed instead to problems with the parameterizations (e.g., cloud, boundary layer, convection schemes, etc.).

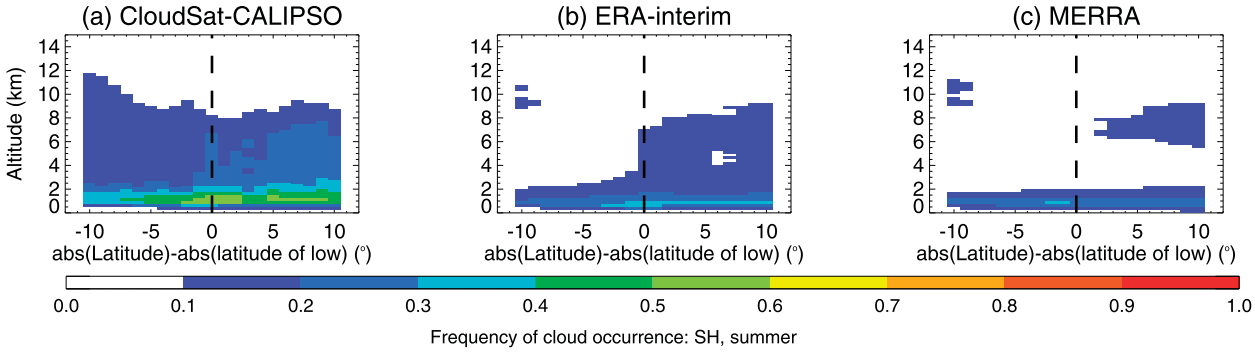

FIG. 8. Composites of cloud vertical distribution along the 7.5°W of and ±10° latitude from the low pressure center, for warm season SH cyclones, in (a) *CloudSat–CALIPSO* observations, (b) ERA-Interim, and (c) MERRA.

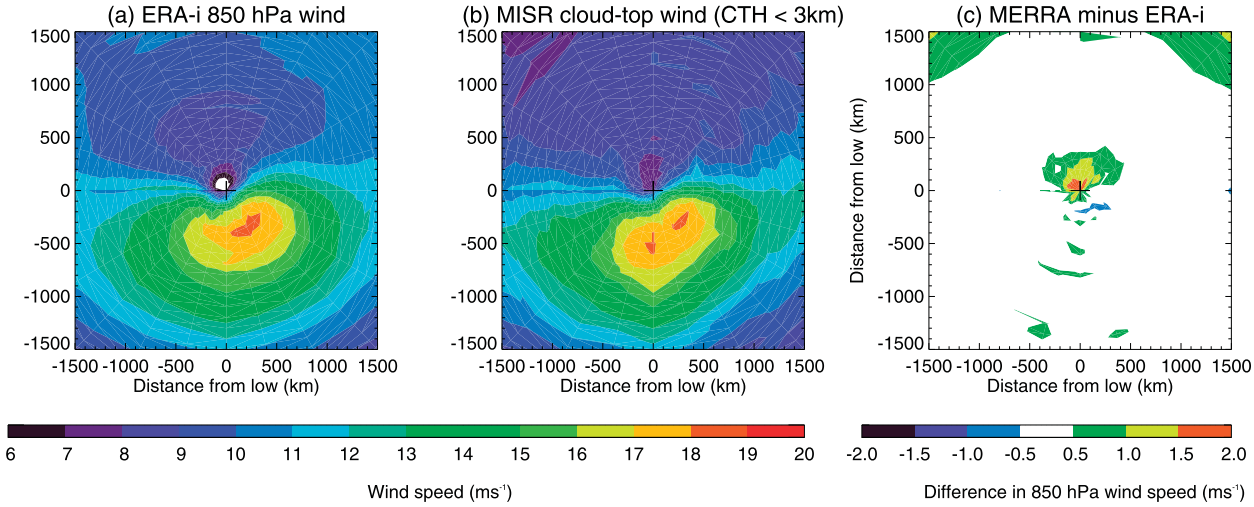

FIG. 9. Cyclone-centered composites of SH warm season (a) ERA-Interim (ERA-i) 850-hPa wind speed, (b) MISR cloud-top wind for tops below 3 km, and (c) difference in 850-hPa horizontal wind between MERRA and ERA-Interim.

b. *Impact of parameterizations*

The atmospheric model used for ERA-Interim is the Integrated Forecast System version 31r1 (IFS; Dee et al. 2011 and references therein) and MERRA is using the Goddard Earth Observing System version 5.2 (GEOS-5; Rienecker et al. 2011 and references therein). [The models are described in greater detail in the online documentation: http://www.ecmwf.int/research/ifsdocs/CY31r1/index.html for IFS and http://gmao.gsfc.nasa.gov/pubs/docs/GEOS5_104606-Vol27.pdf (Rienecker et al. 2008) for GEOS-5. We refer to these documents for the description of the various parameterization schemes discussed below.]

Of importance for low-level cloud cover in these models are (i) the cloud formation and disposal processes (condensation versus erosion and precipitation) parameterized within the cloud scheme, (ii) the planetary boundary layer (PBL) scheme for the occurrence of stratocumulus versus cumulus, and (iii) the shallow convection scheme.

In IFS, clouds form if the grid-average relative humidity exceeds a critical value that changes with altitude. Cloud cover will depend on the departure of the grid-average water mixing ratio from its saturation value and on the rate of decrease of the saturation mixing ratio. In GEOS-5, the cloud cover depends on the departure of the grid-average water mixing ratio from its

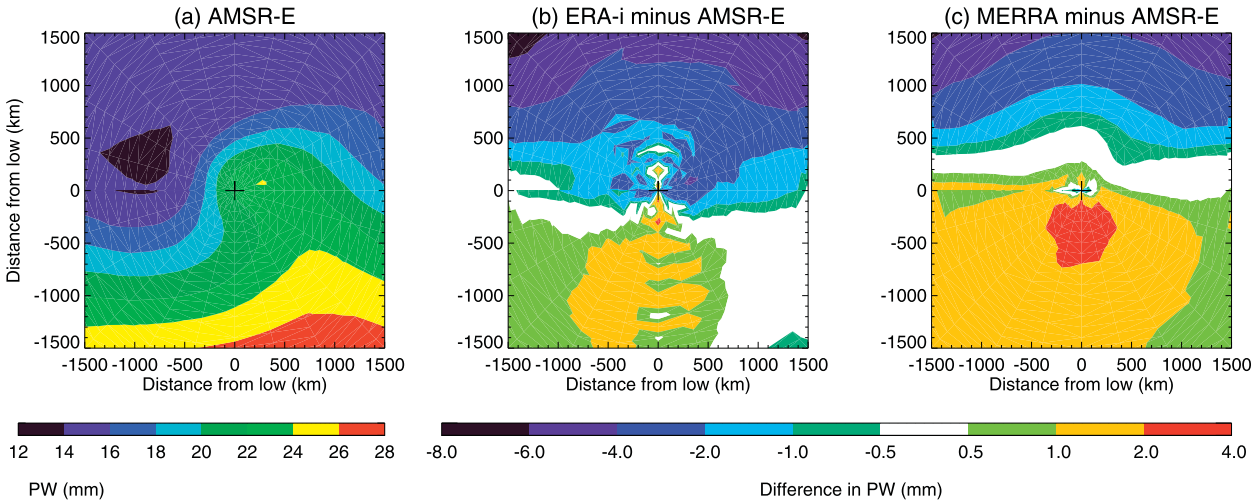

FIG. 10. Cyclone-centered composites of SH warm season (a) AMSR-E PW, difference in PW between (b) ERA-Interim (ERA-i) and AMSR-E and (c) MERRA and AMSR-E.

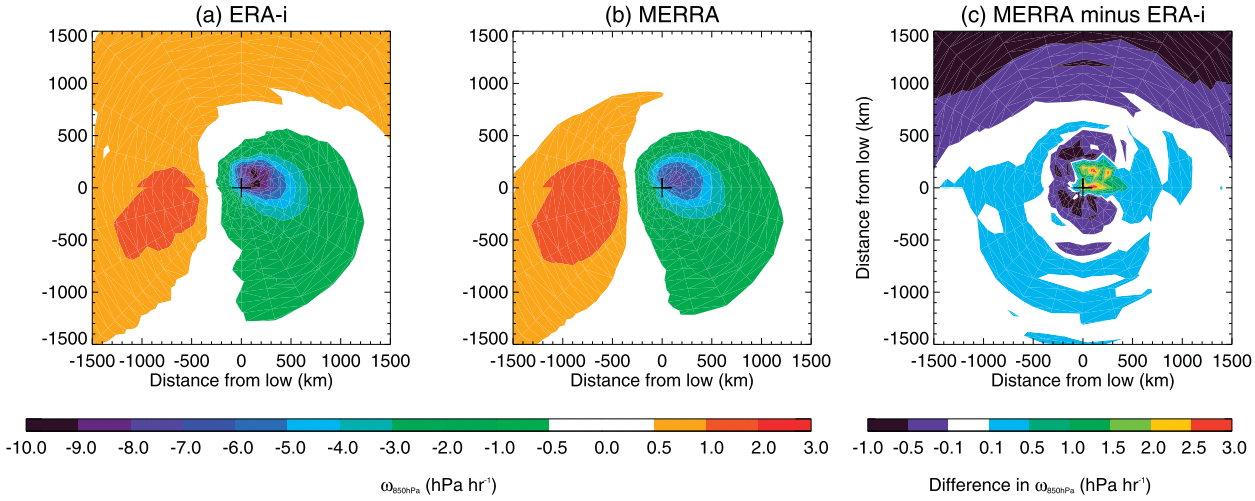

FIG. 11. Cyclone-centered composites of SH warm season 850-hPa vertical velocity for (a) ERA-Interim (ERA-i) and (b) MERRA and (c) difference between MERRA and ERA-Interim in 850-hPa vertical velocity.

saturation value assuming a boxcar probability distribution function of the water mixing ratio. Both schemes allow mixed phase clouds to exist within a fixed temperature range and with the relative amounts of liquid and ice dependent on temperature. However, the temperature at which clouds are fully composed of ice differs: IFS uses 250 K (Tompkins et al. 2007) while GEOS-5 uses 263 K (Bacmeister et al. 2006). This difference in temperature threshold could affect cloud cover as the saturation mixing ratio with respect to ice is lower than that with respect to liquid.

Cloud cover can be affected by cloud erosion: IFS allows cloud erosion through either large-scale and cumulus descent and diabatic heating or through turbulent mixing with unsaturated environmental air. According to the GEOS-5 documentation, cloud erosion is only allowed in ''anvil'' clouds. This cloud type, specific to GEOS-5, results from convective detrainment and is treated separately from large-scale stratiform clouds for 3 h, during which their autoconversion rates are slower and their number densities larger than their stratiform counterparts (Bacmeister et al. 2006). For these clouds, erosion caused by mixing with environmental air is parameterized.

Among the precipitation processes, autoconversion of water to rain is based on the same Sundqvist (1978) parameterization in both IFS and GEOS-5 models, but they treat rain re-evaporation differently. Also, the schemes for autoconversion of ice to snow and ice sedimentation differ. The scheme implemented in GEOS-5 is known to overestimate production of ice precipitation in other models, according to the GEOS-5 documentation.

The PBL scheme and/or its relation with the cloud scheme may participate in the cloud deficiency. For MERRA, GEOS-5 uses the Lock et al. (2000) PBL scheme for unstable or cloud-topped layers and the Louis et al. (1982) scheme for stable layers; and for ERA-Interim, IFS uses an integrated eddy-diffusivity mass flux scheme described by Köhler et al. (2011). Differences between these schemes may imply differences in stratocumulus occurrence (e.g., if the MERRA PBL is shallower than ERA-Interim's or if its inversion is weaker, then it will produce less stratocumulus cloud). Finally, the two convection schemes may simulate a different strength of shallow convection. GEOS-5 uses the Relaxed Arakawa–Schubert (Moorthi and Suarez 1992) convection scheme while IFS relies on the Tiedtke (1989) shallow convection scheme.

The two models use different parameterizations for most of the processes that are involved in low-level cloud cover and it is impossible to easily isolate the root cause for their differences. However, with the observations available to us, we can still examine some aspects of the models and narrow down the possible reasons for such a difference in cloud cover.

First, Fig. 5b shows that average cloud-top temperatures are in the 250–263-K range for most of the western side of the cyclones, and Fig. 10 suggests that moisture amounts are fairly similar between the two reanalyses. If IFS and GEOS-5 used the same parameterization schemes and only the ice temperature thresholds differed, cloud cover would be greater in MERRA than ERA-Interim on the western side of the cyclones. Consequently, the different thresholds for the transition between mixed phase clouds and ice clouds cannot explain the difference in cloud cover between MERRA and ERA-Interim.

Next, we focus on a point 7.5°W and 5° equatorward of the low pressure center (in the region where cloud cover

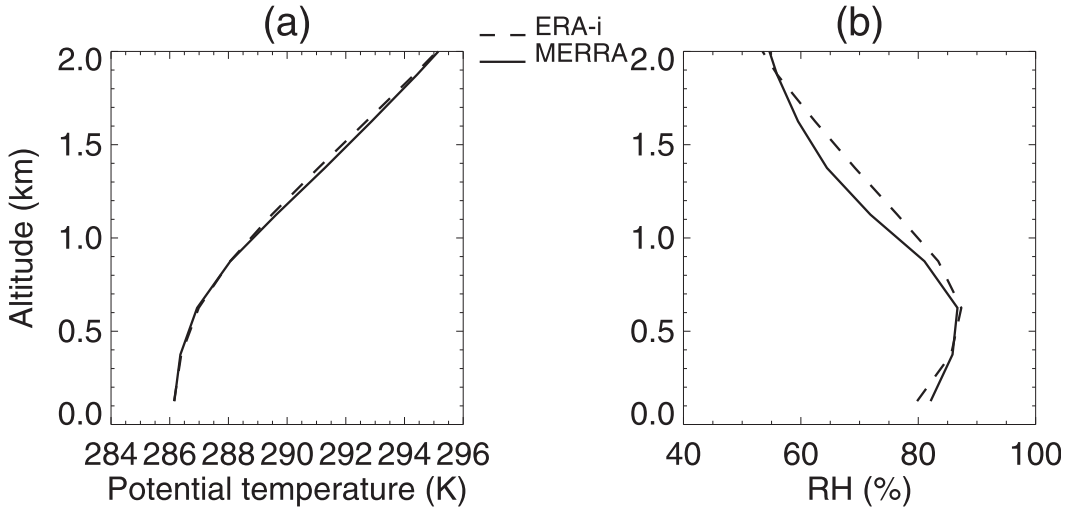

FIG. 12. Profiles of (a) potential temperature and (b) relative humidity (RH) for ERA-Interim (dashed) and MERRA (solid). The profiles are extracted in all SH warm season cyclones, at a point 7.5°W and 5° equatorward of the low pressure centers.

biases are largest), and average MERRA and ERA-Interim potential temperature and relative humidity profiles at this location (Fig. 12). Figure 12a shows that this location exhibits virtually identical potential temperature profiles in the two reanalyses. Therefore, the differences in cloud cover are not related to differences in the temperature vertical structure. There is thus no indication that MERRA produces less stratocumulus clouds because its PBL is shallower or its inversion not as sharp as in the ERA-Interim PBL for the western side of extratropical cyclones. There are no observed soundings available in this region, so it is not possible to tell if this boundary layer structure is realistic.

Figure 12b shows that there are differences in the moisture profiles in the reanalyses (i.e., the ERA-Interim average relative humidity is slightly greater above and lower within the boundary layer than MERRA). This additional moisture in ERA-Interim above the boundary layer could be caused by

- a more efficient erosion process in ERA-Interim. However, Fig. 8 shows slightly greater cloud amounts in ERA-Interim than MERRA at these altitudes, casting some doubt on the importance of cloud erosion processes.
- a potential overestimate in ice precipitation efficiency in MERRA. Unfortunately, this cannot be tested with observations.
- mechanisms that lift moisture above the boundary layer (e.g., shallow convection could be more efficient in ERA-Interim than MERRA).

To test the latter hypothesis further, we examined the Klein and Hartmann (1993) lower-tropospheric static stability (LTS; the difference in potential temperature at 700 hPa minus at the surface). Köhler et al. (2011) indicate that in the IFS PBL scheme the stratocumulus parameterization is used and the convection scheme turned off where LTS $>$ 20 K. The Lock et al. (2000) parameterization used in GEOS-5 also identifies decoupled layers, but we found no mention of the Klein–Hartmann test in MERRA. By calculating and compositing LTS in the two reanalyses, we can verify whether 1) this additional test in IFS can explain additional production of stratocumulus and 2) the range of LTS values in the western side of the cyclones is typical of one specific cloud type.

Figure 13a shows the observed LTS obtained with AIRS 700-mb potential temperature and sea level pressure retrievals and AMSR-E sea surface temperature retrievals. Figures 13b and 13c show the cyclone-centered composite difference in LTS between ERA-Interim and MERRA and the observations. The difference in LTS between the two reanalyses and the observations (Figs. 13b,c) is small, less than 0.2 K, in the area of the cyclone where cloud differences are largest. Therefore, there is no indication that the decoupling test in the IFS model explains the better performance of this model for cloud cover. To further verify this, we also calculate the frequency of occurrence of LTS $>$ 20 K for both reanalysis and look at the difference between the two. Figure 14a shows the frequency of occurrence of LTS $>$ 20 K in ERA-Interim and Fig. 14b in MERRA. Figure 14c shows the difference between MERRA and ERA-Interim frequency of occurrence of LTS $>$ 20 K and confirms that the two reanalyses produce very similar LTS distributions.

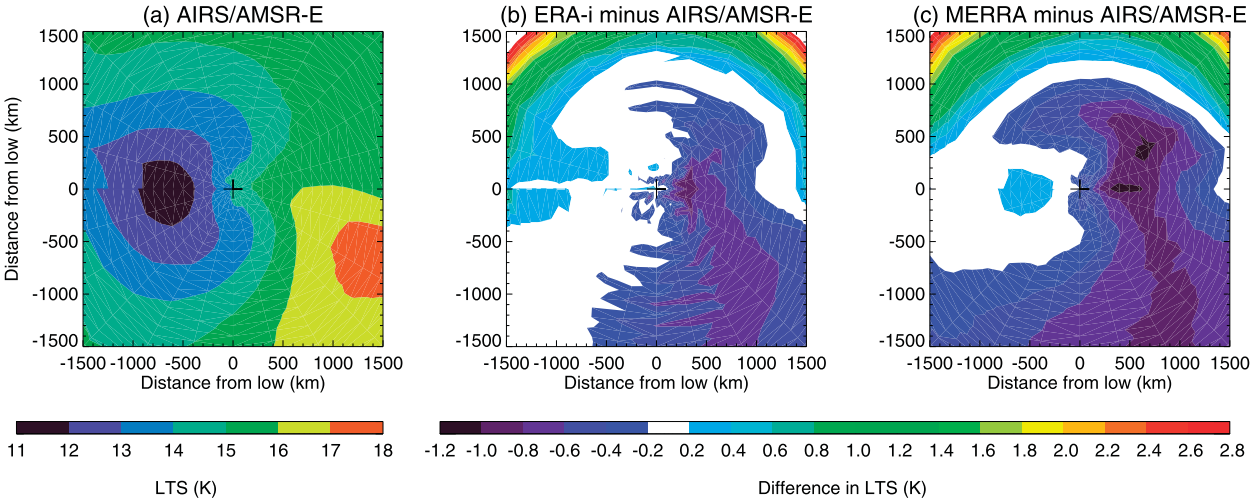

FIG. 13. Cyclone-centered composites of SH warm season of (a) observed LTS calculated using a combination of AIRS and AMSR-E retrievals, and of the difference between (b) ERA-Interim (ERA-i) and the observed LTS and (c) MERRA and the observed LTS.

Figure 13a also indicates that the area of largest difference in cloud cover is also the area where LTS is the lowest: both reanalyses show a region of low frequencies of LTS $>$ 20 K to the west of the cyclones (Figs. 14a,b), with values less than 12%. Consequently, Figs. 13 and 14 suggest that the region where differences in cloud cover between MERRA and ERA-Interim has the largest displays of weak stability. This is consistent with results from Williams et al. (2013) who test various GCMs ability to reproduce surface solar radiation in SH cyclones and find that the largest differences occur for LTS in the 0–20-K range. In addition, MODIS cloud fraction differences in Fig. 6d indicate that this region is often populated by broken clouds. Taken together, these factors suggest that the difference in cloud cover between the reanalysis and with observations could be connected to the shallow convection parameterization (i.e., either the models do not produce cumulus clouds often enough or the cloud amount when present is too low).

7. Conclusions

Our results reveal that even reanalyses, which use a vast array of observations to constrain their model, have difficulty producing the right amount of clouds in the Southern Ocean. We explored cyclone-centered cloud cover composites to establish if this low bias was occurring more readily in certain dynamical situations. We

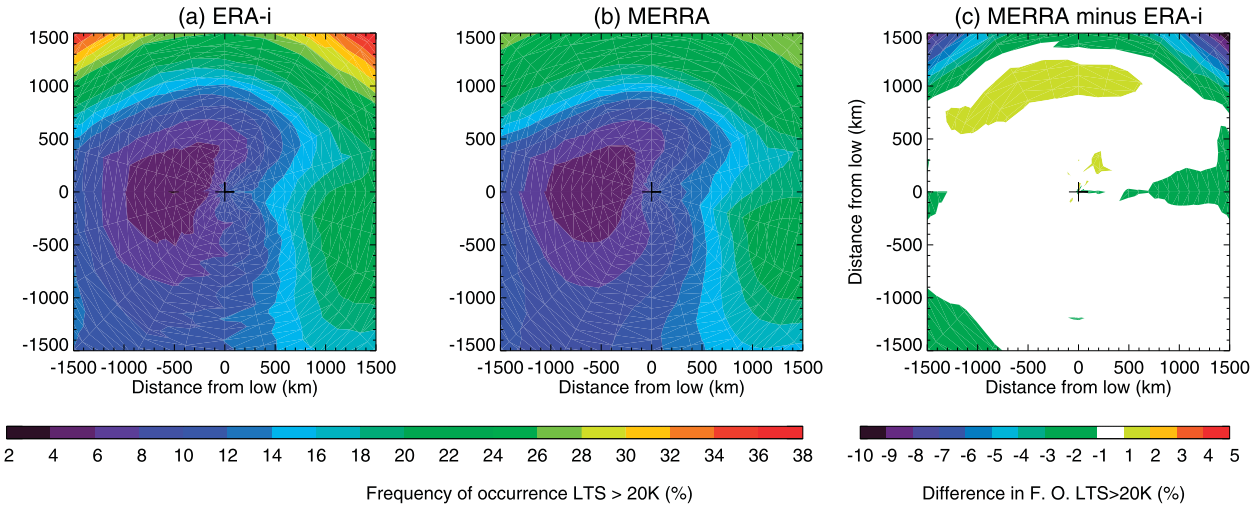

FIG. 14. Cyclone-centered composites of SH warm season frequency of occurrence of LTS $>$ 20 K in (a) ERA-Interim, (b) MERRA, and (c) the difference in frequency of occurrence of LTS $>$ 20 K between MERRA and ERA-Interim.

find that cloud cover in cyclonic environments is underestimated in the ERA-Interim and MERRA reanalyses, especially MERRA, and that this is most acute to the west of the low pressure center. This region of the cyclone displays a subsidence regime and MODIS and MISR cloud-top location retrievals indicate that this is a region where most clouds are at a low level. This is confirmed when examining vertical transects of *CloudSat–CALIPSO* cloud cover to the west of the low pressure center.

Since we found that the MERRA cloud cover bias is larger than that of ERA-Interim, we compared their modeled dynamics and thermodynamics within the cyclones. The large-scale characteristics of the cyclones themselves (850-hPa wind speed and vertical velocity, PW, and temperature) are very similar between the two reanalyses and do not explain differences in their cloud cover. This suggests that the deficiency in both reanalyses' cloud cover and the differences between the two reanalyses are most likely caused by the parameterization schemes used in the underlying models.

We found that the largest difference in cyclone cloud cover between the reanalyses and observations occurs where lower-tropospheric stability is lowest. This is also a region where clouds tend to be of a broken nature. The latter characteristics would suggest that shallow cumulus parameterizations in both reanalyses could be at the origin of the low-level cloud cover bias. Our conjecture that it is the shallow cumulus scheme is reinforced by a recent study showing that although deep convective clouds in MERRA compare well with observations in the tropics (Posselt et al. 2012), some issues with a lack of detrainment at low levels were noted. However, there is no firm indication that shallow convection is the only possible issue. In fact, it is possible that condensation is more efficient in ERA-Interim, and ice removal processes more efficient in MERRA.

The differences in cloud cover cyclone-wide between the reanalyses and MODIS/MISR are consistent with differences found between a GCM and observations by Bodas-Salcedo et al. (2012), in their location and for the cloud level. Bodas-Salcedo et al. (2012) do find some improvement in their GCM low-level cloud cover to the west of the low in SH cyclones when modifying the boundary layer scheme. Williams et al. (2013) also find a correlation between low-level cloud deficiencies at the back of Southern Hemisphere cold fronts in hindcast simulations from a variety of models and their inability to produce the correct amount of surface solar absorption. The Goddard Institute for Space Studies GCM was recently tested with a new boundary layer scheme, which tends to increase the depth of the extratropical boundary layer, and thus permits a larger amount of clouds to be present at low levels. Preliminary tests reveal that the average monthly cloud cover in the Southern Ocean is increased with this new scheme despite the cloud parameterization itself being identical (Yao and Cheng 2012). These different studies and our results all point to model deficiencies for the production of low-level clouds.

Acknowledgments. MODIS data were obtained from the Level 1 and Atmospheric Distribution System at the NASA Goddard Space Flight Center. MISR data files were obtained from the NASA Langley Atmospheric Sciences Data Center. *CloudSat–CALIPSO* GEOPROF-LIDAR data were obtained from the *Cloudsat* Data Processing Center. AMSR-E ocean products were obtained from the National Snow and Ice Data Center. AIRS level-2 files and MERRA files were obtained from the NASA Goddard Earth Sciences Data and Information Services Center. ERA-Interim files were obtained from the European Centre for Medium-Range Weather Forecasts Meteorological Archival and Retrieval System. This work was funded by NASA *CloudSat* Science team Grant NNX10AM20G to CMN and RTOP to ADD, and by NASA the Science of *Terra* and *Aqua* Grant NNX11AH22G to CMN. JFB was funded by a NASA Postdoctoral Program Fellowship. The authors thank the editor, Jay Mace, and two anonymous reviewers for their insightful comments that have helped significantly improve this manuscript.

REFERENCES

Ackerman, S. A., R. E. Holz, R. Frey, E. W. Eloranta, B. C. Maddux, and M. McGill, 2008: Cloud detection with MODIS. Part II: Validation. *J. Atmos. Oceanic Technol.,* **25,** 1073–1086.

Aumann, H. H., and Coauthors, 2003: AIRS/AMSU/HSB on the Aqua mission: Design, science objectives, data products and processing systems. *IEEE Trans. Geosci. Remote Sens.,* **41,** 253–264.

Bacmeister, J. T., M. J. Suarez, and F. R. Robertson, 2006: Rain reevaporation, boundary layer–convection interactions, and Pacific rainfall patterns in an AGCM. *J. Atmos. Sci.,* **63,** 3383–3403.

Bauer, M., and A. D. Del Genio, 2006: Composite analysis of winter cyclones in a GCM: Influence on climatological humidity. *J. Climate,* **19,** 1652–1672.

Bodas-Salcedo, A., and Coauthors, 2011: COSP satellite simulation software for model assessment. *Bull. Amer. Meteor. Soc.,* **92,** 1023–1043.

——, K. D. Williams, P. R. Field, and A. P. Lock, 2012: The surface downwelling solar radiation surplus over the Southern Ocean in the Met Office model: The role of midlatitude cyclone clouds. *J. Climate,* **25,** 7467–7486.

Booth, J. F., C. M. Naud, and A. D. Del Genio, 2013: Diagnosing warm frontal cloud formation in a GCM: A novel approach using conditional subsetting. *J. Climate,* **26,** 5827–5845.

Bosilovich, M. G., F. R. Robertson, and J. Chen, 2011: Global energy and water budgets in MERRA. *J. Climate,* **24,** 5721–5739.

Dee, D. P., and Coauthors, 2011: The ERA-Interim reanalysis: Configuration and performance of the data assimilation systems. *Quart. J. Roy. Meteor. Soc.,* **137,** 553–597.

Di Girolamo L., A. Menzies, G. Zhao, K. Mueller, C. Moroney, and D. J. Diner, 2010: Level 3 cloud fraction by altitude algorithm theoretical basis. JPL Tech. Doc. D-62358, 18 pp.

Diner, D. J., and Coauthors, 1998: Multi-Angle Imaging Spectroradiometer (MISR) instrument description and experiment overview. *IEEE Trans. Geosci. Remote Sens.,* **36,** 1072–1087.

Field, P. R., and R. Wood, 2007: Precipitation and cloud structure in midlatitude cyclones. *J. Climate,* **20,** 233–254.

——, A. Gettelman, R. B. Neale, R. Wood, P. J. Rasch, and H. Morrison, 2008: Midlatitude cyclone compositing to constrain climate model behavior using satellite observations. *J. Climate,* **21,** 5887–5903.

Haynes, J. M., C. Jakob, W. B. Rossow, G. Tselioudis, and J. Brown, 2011: Characteristics of Southern Ocean cloud regimes and their effects on the energy budget. *J. Climate,* **24,** 5061–5080.

Hewson, T. D., 1998: Objective fronts. *Meteor. Appl.,* **5,** 37–65.

Hodges, K. I., R. W. Lee, and L. Bengtsson, 2011: A comparison of extratropical cyclones in recent reanalyses ERA-interim, NASA MERRA, NCEP CFRS, and JRA-25. *J. Climate,* **24,** 4888–4906.

Kawanishi, T., and Coauthors, 2003: The Adanced Microwave Scanning Radiometer for the Earth Observing System (AMSR-E), NASDA's contribution to the EOS for global energy and water cycle studies. *IEEE Trans. Geosci. Remote Sens.,* **41,** 184–194.

Klein, S. A., and D. L. Hartmann, 1993: The seasonal cycle of low stratiform clouds. *J. Climate,* **6,** 1588–1606.

Köhler, M., M. Ahlgrimm, and A. Beljaars, 2011: Unified treatment of dry convective and stratocumulus-topped boundary layers in the ECMWF model. *Quart. J. Roy. Meteor. Soc.,* **137,** 43–57.

Lock, A. P., A. R. Brown, M. R. Bush, G. M. Martin, and R. N. B. Smith, 2000: A new boundary layer mixing scheme. Part I: Scheme description and single column model tests. *Mon. Wea. Rev.,* **128,** 3187–3199.

Loeb, N. G., B. A. Wielicki, D. R. Doelling, G. L. Smith, D. F. Keyes, S. Kato, N. Manalo-Smith, and T. Wong, 2009: Toward optimal closure of the earth's top-of-atmosphere radiation budget. *J. Climate,* **22,** 748–766.

Louis, J., M. Tiedtke, and J. Geleyn, 1982: A short history of the operational PBL-parameterization at ECMWF. *Proc. ECMWF Workshop on Planetary Boundary Layer Parameterization,* Reading, United Kingdom, ECMWF, 59–79.

Mace, G. G., Q. Zhang, M. Vaughan, R. Marchand, G. Stephens, C. Trepte, and D. Winker, 2009: A description of hydrometeor layer occurrence statistics derived from the first year of merged CloudSat and CALIPSO data. *J. Geophys. Res.,* **114,** D00A26, doi:10.1029/2007JD008755.

Marchand, R., G. G. Mace, T. Ackerman, and G. Stephens, 2008: Hydrometeor detection using *CloudSat*—An Earth-orbiting 94-GHz cloud radar. *J. Atmos. Oceanic Technol.,* **25,** 519–533.

Moorthi, S., and M. J. Suarez, 1992: Relaxed Arakawa–Schubert: A parameterization of moist convection for general circulation models. *Mon. Wea. Rev.,* **120,** 978–1002.

Moroney, C., R. Davis, and J.-P. Muller, 2002: Operational retrieval of cloud-top heights using MISR data. *IEEE Trans. Geosci. Remote Sens.,* **40,** 1532–1540.

Naud, C. M., A. D. Del Genio, and M. Bauer, 2006: Observational constraints on the cloud thermodynamic phase in midlatitude storms. *J. Climate,* **19,** 5273–5288.

——, ——, ——, and W. Kovari, 2010: Cloud vertical distribution across warm and cold fronts in *CloudSat*–CALIPSO data and a general circulation model. *J. Climate,* **23,** 3397–3415.

——, D. J. Posselt, and S. C. van den Heever, 2012: Observational analysis of cloud and precipitation in midlatitude cyclones: Northern versus Southern Hemisphere warm fronts. *J. Climate,* **25,** 5135–5151.

——, J. F. Booth, D. J. Posselt, and S. C. van den Heever, 2013: Multiple satellite observations of cloud cover in extratropical cyclones. *J. Geophys. Res. Atmos.,* **118,** 9982–9996, doi:10.1002/jgrd.50718.

Platnick, S., M. D. King, S. A. Ackerman, W. P. Menzel, B. A. Baum, J. C. Riedi, and R. A. Frey, 2003: The MODIS cloud products: Algorithms and examples from *Terra*. *IEEE Trans. Geosci. Remote Sens.,* **41,** 459–473.

Posselt, D. J., A. R. Jongeward, C.-Y. Hsu, and G. L. Potter, 2012: Object-based evaluation of MERRA cloud physical properties and radiative fluxes during the 1998 El Niño–La Niña transition. *J. Climate,* **25,** 7313–7327.

Rienecker, M. M., and Coauthors, 2008: The GEOS-5 data assimilation system—Documentation of versions 5.0.1, 5.1.0, and 5.2.0. NASA Tech. Rep. Series on Global Modeling and Data Assimilation NASA/TM-2008-104606, Vol. 27, 118 pp. [Available online at http://gmao.gsfc.nasa.gov/pubs/docs/GEOS5_104606-Vol27.pdf.]

——, and Coauthors, 2011: MERRA: NASA's Modern-Era Retrospective Analysis for Research and Applications. *J. Climate,* **24,** 3624–3648.

Salomonson, V. V., W. L. Barnes, P. W. Maymon, H. E. Montgomery, and H. Ostrow, 1989: MODIS: Advanced facility instrument for studies of the earth as a system. *IEEE Trans. Geosci. Remote Sens.,* **27,** 145–153.

Stephens, G. L., and Coauthors, 2002: The CloudSat mission and the A-Train: A new dimension to space-based observations of clouds and precipitation. *Bull. Amer. Meteor. Soc.,* **83,** 1771–1790.

Sundqvist, H., 1978: A parameterization scheme for non-convective condensation including prediction of cloud water content. *Quart. J. Roy. Meteor. Soc.,* **104,** 677–690.

Tiedtke, M., 1989: A comprehensive mass flux scheme for cumulus parameterization in large-scale models. *Mon. Wea. Rev.,* **117,** 1779–1800.

Tompkins, A. M., K. Gierens, and G. Rädel, 2007: Ice supersaturation in the ECMWF integrated forecast system. *Quart. J. Roy. Meteor. Soc.,* **133,** 53–63.

Trenberth, K. E., and J. Fasullo, 2010: Simulation of present-day and twenty-first-century energy budgets of the Southern Oceans. *J. Climate,* **23,** 440–454.

Wentz, F., and T. Meissner, 2004 AMSR-E/Aqua L2B global swath ocean products derived from Wentz algorithm, version 2. National Snow and Ice Data Center, Boulder, CO, digital media. [Available online at http://nsidc.org/data/ae_ocean.html.]

Williams, K. D., and Coauthors, 2013: The transpose-AMIP II experiment and its application to the understanding of Southern Ocean cloud biases in climate models. *J. Climate,* **26,** 3258–3274.

Winker, D. M., M. A. Vaughan, A. H. Omar, Y. Hu, K. A. Powell, Z. Liu, W. H. Hunt, and S. A. Young, 2009: Overview of the CALIPSO mission and CALIOP data processing algorithms. *J. Atmos. Oceanic Technol.,* **26,** 2310–2323.

Yao, M.-S., and Y. Cheng, 2012: Cloud simulations in response to turbulence parameterizations in the GISS Model E GCM. *J. Climate,* **25,** 4963–4974.